

Imaging Myocardial Strain

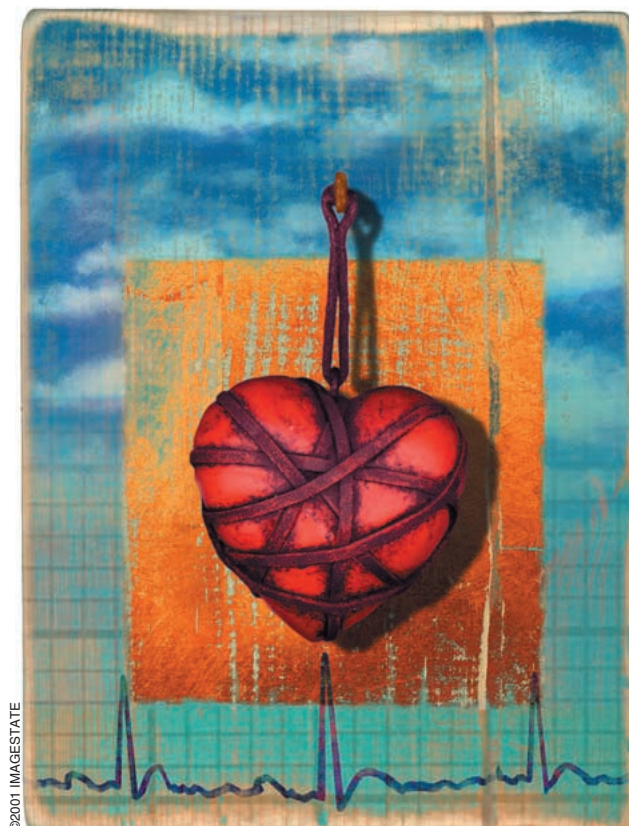
Elliot McVeigh and Cengizhan Ozturk

The heart is a spectacularly successful electromechanical pump that provides highly tuned cardiac output. Its failure, however, is by far the leading cause of death in the western world; in the United States alone, approximately 1/2 million people die each year due to cardiovascular disease, which represents 1/5 of all deaths. There are over 1 million new and recurrent cases of coronary attack each year [2].

Many of these fatalities are from "sudden death," which is a catastrophic breakdown in the normal coherent electrical depolarization of the heart and hence a total decoupling of the electrical activation with a coherent mechanical pressure pulse. It has been impossible to predict if a specific heart will succumb to this catastrophic transition. The coupling of the mechanical contraction of the heart to the coherent electrical activation is critical for normal performance of the ventricles; however, the precise relationship between these two dynamic processes is difficult to measure. The measurement of the electrical activity of the heart is a very mature field. Body surface electrode mapping [16], [17], [42], intracavity electrodes [41], optical techniques [63], and monophasic action potentials [31] are just some of the methods used to map myocardial electrical activity.

Measuring the local mechanical activity of the heart has lagged behind the measurement of electrical activity due to a lack of measurement tools. Myocardial wall motion abnormalities have been studied for years in the context of regional ischemia [15], [36]. Implanted beads [26], [67] and screws [35] have been used to measure the mechanical activity of the heart in a few isolated regions. Over the past decade, precise and accurate methods for

measuring local three-dimensional (3-D) myocardial motion with magnetic resonance imaging (MRI) have been developed using presaturation tagging patterns [8], [73], velocity encoded phase maps [58], [68], and displacement encoded phase maps [1], [55]. Concurrently, the quality of cardiac MRI images improved greatly with the use of customized receiver coils [14], [19], [20] and the speed of acquisition has increased dramatically with the advent of undersampling techniques [5], [43], [61] and new generations of MR machines with faster switching gradient coils. The use of these cardiac MRI techniques to produce an image of the local deformation of the heart in the form of a myocardial strain image will be described in this article. Using these images, the "mechanical activation" of the heart will be defined, that is, the time of onset of contraction. A map of the mechanical activation over the heart is a direct analogy to an electrical activation map of the heart.



Cardiac Imaging

MR cardiac imaging is generally performed using cardiac gating to synchronize data acquisition to the beating heart: data are collected over 1-32 heartbeats (depending on the application). The raw data are partially collected during each cardiac cycle, and the complete data set is pieced together from a number of beats (which are assumed to have identical motions).

The assessment of myocardial wall motion with the precise quantification of regional myocardial contraction requires high quality MR images of the heart. However, a number of physical attributes make the heart a difficult

object to image. Motion of the blood in the heart chambers may cause severe image artifacts due to velocity-induced signal changes that do not repeat from beat to beat. The motion of the diaphragm during patient breathing can move the heart on the order of 2-3 cm during data acquisition causing both blurring and motion ghosts. For this reason, most cardiac imaging techniques are performed during a patient breath-hold. Lastly, the motion of the heart wall itself is on the order of 2.5 cm/s during systole and 10 cm/s during rapid filling; because this is the motion that we are trying to measure in assessing cardiac contractile function, the sampling rate must be sufficient to avoid motion blurring. An example of two frames from a “movie” of cardiac contraction is shown in Fig. 1.

Cardiac Tagging Techniques

The principle of “tagging” or marking nuclear spins was first proposed by Morse and Singer for measuring bulk flow [51]. They showed that the application of a “pre-saturation” radio-frequency (RF) pulse delivered upstream in a flowing fluid could be observed as a transient drop in signal intensity when the “tagged” fluid moved through the MR detector. It was demonstrated by Zerhouni et al. that the same principle could be used in MR imaging to visually mark tissue with thin planes of saturated magnetization to measure the more complex deformations of the heart [73]. Cardiac tagging therefore uses this simple principle: the underlying object is multiplied with a known intensity function and the volume is imaged after some time delay; the change in shape of the intensity pattern in the image reflects the change in shape of the underlying object containing the intensity pattern. An obvious intensity pattern to track is a Cartesian grid of lines; in 1989 Axel and Dougherty proposed a very efficient scheme for generating a large set of parallel planes of saturation throughout the entire imaging volume [7], [8] to produce such a grid.

We can break down the process of cardiac tagging into three stages:

- ▲ 1) a saturation pattern is placed in the myocardial tissue with spatially selective RF pulses;
- ▲ 2) a sequence of MR images is obtained in which the motion of the saturation pattern can be observed;
- ▲ 3) the motion of the saturation pattern is used to solve for the motion of the myocardium.

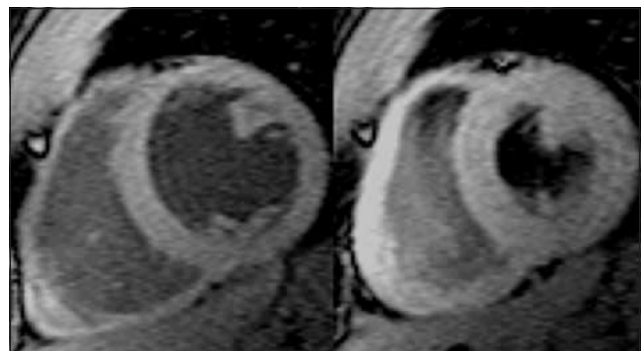
Fig. 2 shows the same heart as in Fig. 1, only in this case the patient’s electrocardiogram (ECG) triggers the scanner to play out a set of RF and gradient pulses which create a tagging pattern before imaging. The parallel tagging lines appear in the first time frame, and their deformation is evident in subsequent movie frames.

Many tagging patterns have been proposed for imaging myocardial deformation: starburst radial tags [46], parallel line patterns [8], tagging grids [8], [47], [52], striped radial tags [13], sinc modulated comb functions [12], and contrast enhanced difference patterns [30]. Ex-

tensive efforts have been directed towards validating these patterns for measuring deformation with phantom experiments of both stationary [4], [71] and moving samples [50]. As will be demonstrated below, the parallel-line tagging pattern is attractive because of its compact Fourier spectrum.

Imaging Tagged Magnetization

For the majority of data acquisition schemes, the raw data for MR images are collected as straight line samples of the Fourier domain; therefore, the correspondence between the spatial frequency components of the tagging pattern and the spatial frequencies sampled by the imaging sequence deserves special consideration. To image the temporal evolution of myocardial strain we are required to track the position of the tagging pattern over time; therefore, the data acquisition scheme should be designed to sample rapidly the Fourier components that are most important for resolving the tagging pattern. For example, if the tags are a set of lines parallel to the y axis, the Fourier components of this pattern will be highly concentrated along the k_x axis in k-space [44]. (Note: Fourier space is often called “k-space” in MR after the spatial frequency variables k_x , k_y , k_z .) Fig. 3 shows an example of this principle. From this figure it is clear that the optimal method

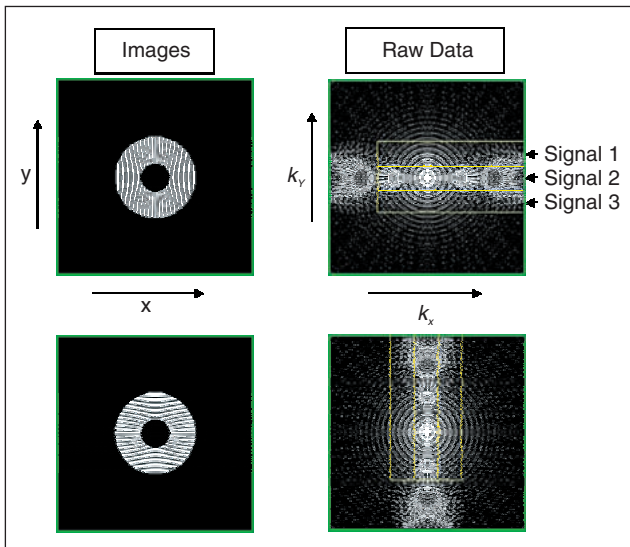


▲ 1. Two time frames from a movie of a short axis section of a normal heart. These images were obtained in 16 heartbeats by gating the MRI acquisition to the patient’s ECG. During the acquisition the patient was required to hold his breath.

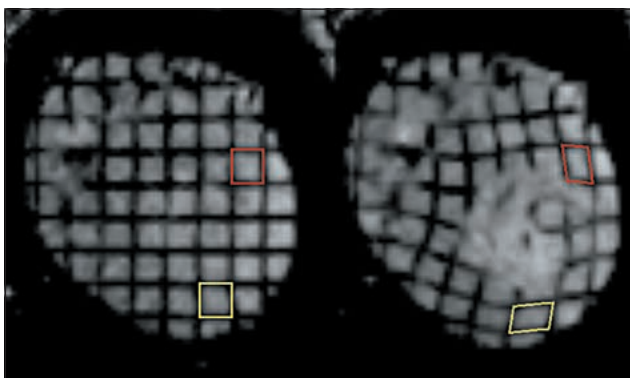


▲ 2. Two time frames from the same heart obtained with a tagged MRI study. At end-diastole (left frame) a parallel plane saturation pattern is placed in the heart. This provides physical markers which can be used to track motion as the heart moves.

of imaging this pattern is by rapidly reading out the Fourier data in the horizontal direction. In MRI, this is accomplished by applying the “readout” gradient along the k_x axis. To measure the displacement in the orthogonal direction *both* the tags and readout gradient should rotate 90°, as shown in the lower part of Fig. 3. In the figure, most of the power is concentrated along the central axes of the Fourier space. An efficient way to sample this data is to segment it into three readout windows, labeled Signal 1-3 above. Two separate acquisitions with orthogonal parallel-line tagging patterns, and orthogonal data readout windows, give a compact data set. The combined images provide equivalent sampling to a grid pattern of tags, but with higher resolution in the directions perpendicular to the tags. The fact that we can use a rectangular sampling window in Fourier space means that time resolution can be improved and that the total acquisition time can be



▲ 3. The two images on the left show prototypes of the signal from tagged myocardium after contraction of the ventricle. The squares on the right show the logarithm of the Fourier power spectrum of the images on the left.



▲ 4. Two time frames in the cardiac cycle in a heart that is being paced from the apex of the right ventricle. The left time frame is immediately after the tags have been placed, and the right time frame is shortly after the pacing stimulus has been applied. The red and yellow boxes indicate circumferential stretching and radial compression.

reduced. For cardiac imaging in patients, this means a shorter breath-hold time. Typical breath-hold acquisitions are obtained in under 15 s, and the images have voxel dimensions on the order of 1.2 mm × 2 mm × 7 mm. Each time frame in the temporal sequence is separated by 25-50 ms, and the tags are usually placed 6-7 pixels apart along the higher resolution readout direction.

Although tagging pulses can be appended to any imaging sequence, the imaging sequence must provide good contrast between the tagged and nontagged myocardium and provide the temporal and spatial resolution required to track the saturation patterns. “Segmented k -space” techniques [5], [27], [44], [62] offer a good compromise between artifact reduction and good contrast-to-noise between the tags and myocardium. For an excellent description of fast imaging techniques appropriate for imaging the heart, the reader should consult a comprehensive text on MRI written for the signal processing audience [33], [40].

Computation of Strain Images

Analysis of Tagged Images

The objective of the analysis of tagged images is to obtain an estimate of the six components of the strain tensor at each point in the myocardium, at each time during the heart cycle. The strain tensor characterizes the *local* deformation of the myocardium, which is a measure of myocardial performance. Bulk translations and rotations of the entire heart may actually dominate the displacement and velocity measurements, but these are of limited value as an index of local myocardial contraction. Fig. 4 shows the basic principle of measuring the local deformation with MR tagging. The concept of local myocardial deformation is simple to appreciate by observing the change in shape of the squares superimposed on the images; the change in shape is quantified with a strain tensor.

Estimation of Local Myocardial Strains

To obtain precise quantification of the regional displacements and strains, the position of the tags must be measured with a “tag detection” algorithm [4], [32], [39], [47], and the 3-D motions of the tissue computed from the combination of partial displacement information from each tag. Tag detection is extremely precise and accurate [4], [47], [50], [71]. For example, it has been demonstrated with simulations and experiments that the position of the center of a single Gaussian-shaped tag can be estimated to within 0.1 pixels if the contrast-to-noise ratio is greater than ten and the tag has a full-width at half maximum of 1.5 pixels [4]. It has been shown also that the precision of tag detection is not a sensitive function of tag shape [4].

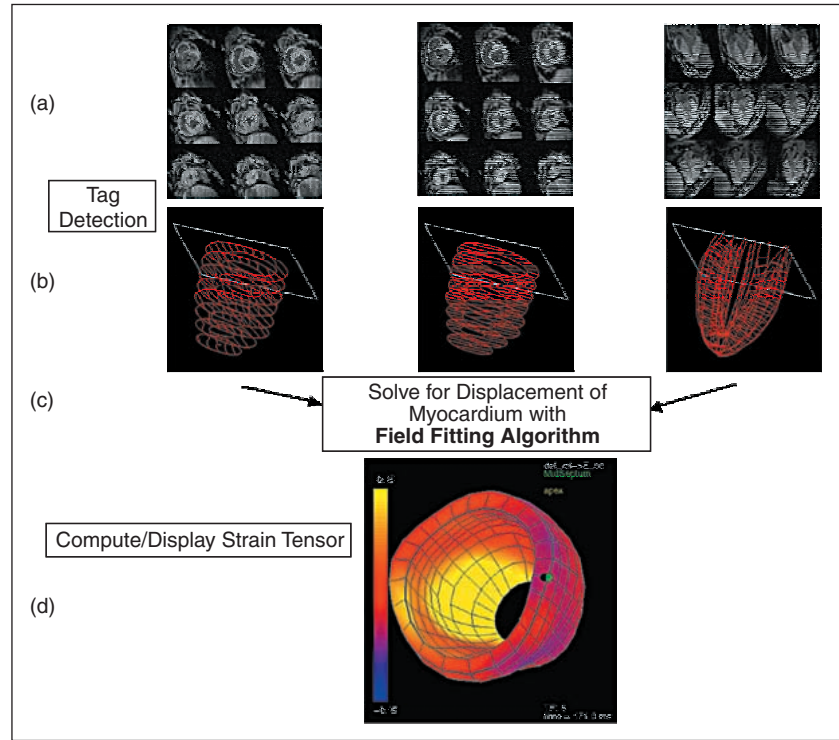
Once the relative position of the tags has been characterized by a string of detected tag points lying along the tag line, these data can be used to estimate the 3-D displacement field of the myocardium and then calculate the strain

at each point in the myocardium. A number of approaches can be employed to perform this estimation. The tag data can be interpolated to solve iteratively for a set of discrete displacements [49], the data can be used to solve for low-order basis functions in finite element models of the heart [70], or the displacement field of the entire left ventricle can be fit using all of the available data [23], [53], [54]. Recently parameter-free models of left ventricular strain have been developed [25], as well as field models based on B-splines [3], [56]. Each of these methods has different tradeoffs between the stability of the solution, and the spatial resolution of the strain field [23]. Fig. 5 outlines the process of fitting displacement field to a set of images. For all of these methods, it is important to understand what information is provided by the tag data: a point on a tag only gives the displacement of that point in the direction perpendicular to the original tag plane, as shown in Fig. 6. Therefore, after detection of all of the image points that lie within the tag lines, the complete data set comprises a list of 1-D displacements, measured on a set of fixed imaging planes. As an example of one of these methods for calculating 3-D displacement fields, we now look more closely at the B-spline method as described by Ozturk [56].

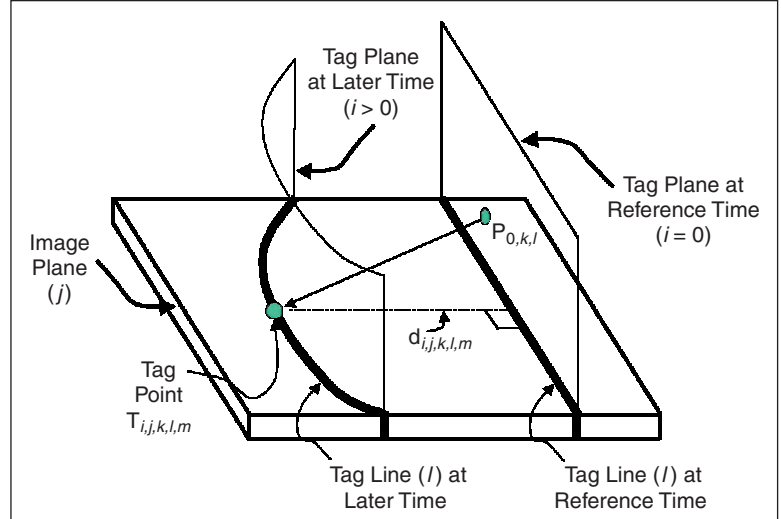
Inverse Motion Field Fitting with B-Splines

For the example described in this section, we will use a data geometry shown in Fig. 7. Three separate tagged data sets are shown in this figure: 1) a short-axis image plane with tags at 45°, 2) a short-axis image plane with tags at 135°, and 3) a long-axis image plane with tags oriented parallel to the short-axis image planes. For a given short axis plane (j) and time frame (i), we have separate displacement information coming from the two sets of parallel plane tags; we refer to each set of tags as a tag “stack.” For each tag stack (k), tag points, T , can be indexed by tag plane (l), and location along a given tag line (m) as shown in Fig. 6. Using this notation the 1-D tag displacement d at a tag point T can be written as

$$d_{i,j,k,l,m} = (\bar{T}_{i,j,k,l,m} - \bar{P}_{0,k,l}) \cdot \vec{N}_k \quad (1)$$



▲ 5. A schematic diagram of the steps involved in computing the strain tensor over the whole left ventricle. (a) The tagged images for multiple slices at a single time frame are acquired. (b) The tags are segmented in the images, yielding a set of curves in three-space sampling the 1-D projections of the deformations of the tag planes. (c) These 1-D projections are used to interpolate the 3-D trajectories of specific material points in the myocardium, i.e., create a displacement field over the myocardium. (d) The 3-D trajectories or displacement field are used to compute the component values of the strain tensor at each point on the left ventricle. The values are then available to display as a color overlay on the model of the points.



▲ 6. A schematic diagram showing the features of the tag tracking data within a specific image plane. The indexes for the tag point T , correspond to those used in (1). The shape of a tag plane, labeled with the index l , is shown at two times: the reference time ($i = 0$) when the plane is flat, and a later time ($i > 0$) when the tag plane has moved and also become bent. A set of “tag points” can be detected along the tag line, and these tag points can be indexed within a tag line with the counter m . We measure the 3-D position of the tag point T . We know the position of the reference tag plane, therefore we know the normal distance, d , from that tag plane to T . We do not know the starting position of the tag point P .

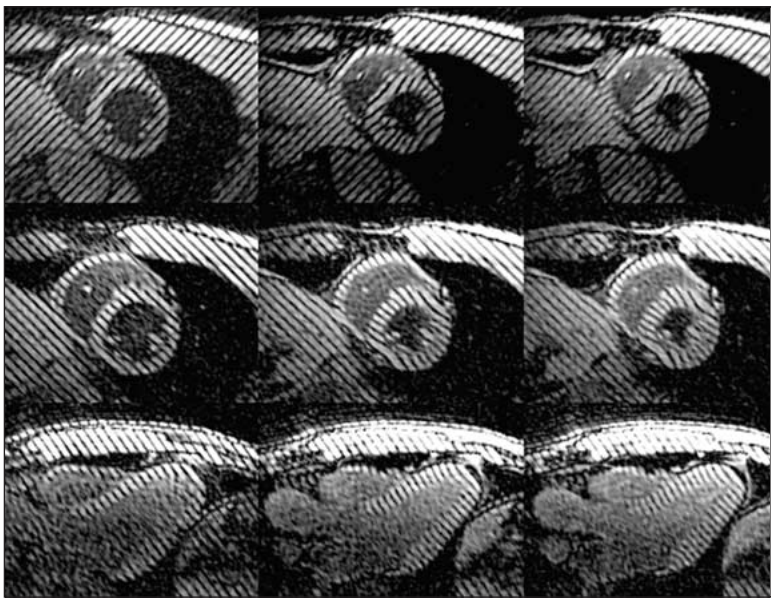
where

- ▲ i is time frame ($1 \leq i \leq 20$);
- ▲ j is short axis image plane ($1 \leq j \leq 10$, for slices from the base to apex);
- ▲ k is tag stack ($1 \leq k \leq 2$, for the 45° and 135° tags as shown in Fig. 4);
- ▲ l is tag plane index;
- ▲ m is the index for each point along the tag line;
- ▲ $P_{0,k,l}$ is a point on tag plane l of stack k at the reference time;
- ▲ N_k is the unit normal of the tag plane k ;
- ▲ (\bullet) is the dot product.

Each tag point, T , has three coordinates in the image-based coordinate system, and as shown in (1), the information it gives is the perpendicular displacement, d , of the tag plane from its original location. For each short-axis image plane, time frame, and short-axis tag stack, we formulate a 2-D B-spline tensor field to fit a smooth field of these perpendicular displacements:

$$\hat{d}_{i,j,k} = \sum_u \sum_v B_u(x) B_v(y) \cdot C_{i,j,k,u,v}. \quad (2)$$

In this equation, B represents a B-spline basis function, x and y are image coordinates, u and v are B-spline parameters, and C are control point values. Summation is done over all the defined control point 2-D tensor products for a given xy -location. The basis function for a given location is calculated from the homogenous knot sequence of the corresponding desired control point number and de-



▲ 7. An array of images showing three orthogonal tagging patterns in the heart. The two short axis movies shown in the top two rows give displacement in the short axis plane. The top row has a "tag stack" with an orientation of 45° , the middle row has a separate tag stack with an orientation of 135° . The long axis movie in the bottom row shows the displacement of the base of the heart towards the apex. The orientation of the short axis imaging plane corresponds to the orientation of one of the tagging planes shown in the bottom row. Data such as this long axis image is used to measure the "through plane" motion that is missed in the top two rows.

gree of the B-spline using the standard iterative formula [22]. We have chosen cubic splines, and several densities of 2-D control point grids have been employed. The control points for a given short-axis image plane, tag direction, and time frame are determined using least squares with peripheral conditioning [56]. If the imaging data has 20 time frames, ten short-axis image planes, and two short-axis tag stacks, then 400 independent tag displacement fields are computed for each set.

We have a B-spline parametric representation, so we can calculate the tag displacement value at any image point using (2). If we evaluate the field at the original tag points, we can compute the absolute difference between calculated and observed displacements as the tag displacement residual error [56]. This can be done for a range of control point densities to optimize the fit.

After calculating displacement fields of both tag stacks at a given short-axis image plane and time frame, we can determine two components of the past total trajectory of any tag point. If care is taken to use the same region of interest in both short-axis tag displacement fields for a given short-axis image, we can describe a single 2-D inverse deformation field (U):

$$U_{i,j} : \mathbf{R}^2 \longrightarrow \mathbf{R}^2$$

$$\vec{D}_{i,j} = \sum_u \sum_v B_u(x) B_v(y) \cdot \begin{bmatrix} C_{i,j,1,u,v} \\ C_{i,j,2,u,v} \end{bmatrix}. \quad (3)$$

This is similar to (2), but the final displacement is now a 2-D vector. For any point, on a given short-axis image plane and time frame, the result of this inverse field is a 2-D vector pointing to the planar projection of its reference point to the current image plane.

Through-Plane Motion Field Fitting

The final inverse motion field should map each tag point to its reference location at the reference time, and the missing component of this motion in (3) is the motion that is perpendicular to the short-axis, which can be computed using long-axis images. A long-axis image plane is shown at different times in the bottom panel of Fig. 7. The steps to this process are: 1) 2-D B-spline field fit for the tag displacement at each long-axis plane, 2) evaluation of the long-axis parametric fields at each short-axis image plane intersection line, and 3) a field fit at each short-axis plane using the through plane motion information coming from step 2.

The first and last steps are essentially identical to the short-axis in-plane tag displacement field fitting of the previous section. At the end of step 2, we have a radial sampling of through plane motion at short-axis imaging planes [56]. We can now describe a 3-D inverse field:

$$U_{i,j} : \mathbb{R}^2 \longrightarrow \mathbb{R}^3 \quad (4)$$

$$\vec{D}_{i,j} = \sum_u \sum_v B_u(x) B_v(y) \cdot \begin{bmatrix} C_{i,j,1,u,v} \\ C_{i,j,2,u,v} \\ C_{i,j,3,u,v} \end{bmatrix}.$$

Forward Motion Field Fitting

The result of the fitting procedure in the previous section is a vector field, which maps any point found in the image planes back to its starting location. Since imaging planes are fixed and the heart is moving through this plane during imaging, tag displacements measured at the same image location but at different time frames point back to different *material points* in the myocardium. We define the cardiac material points by their positions in a volume of interest at the reference time.

Three-dimensional inverse displacement vectors of all the corresponding short-axis tag points are calculated using (4). These displacement vectors map tag points to their material locations at the reference time. Conversely, for every time frame, the forward transformation should bring the material points back to their corresponding tag point locations. The forward deformation for a given time frame (i) can be described as a three-dimensional B-spline tensor product

$$\phi(P_i) = \sum_u \sum_v \sum_w B_u(\tilde{x}_i) B_v(\tilde{y}_i) B_w(\tilde{z}_i) \cdot \vec{C}_{u,v,w,i}. \quad (5)$$

In this equation, the sum for a given material is done over the 3-D-tensor product of basis functions and control points. The basis functions for a given location are calculated, as before, using the corresponding knot sequence and degree of the B-spline, and the control points for each time frame are found by least square minimization. We distinguish material from image based coordinates with the use of symbol (~). The result of this motion field is not the coordinates of the new location but a vector pointing to the new location from the material point P . After the 3-D forward deformation field is constructed for each time frame, a smoothing of control point values is performed over time. For this we have used cubic splines and seven control points. Time smoothing parameters have been kept constant when different densities of spatial control points were evaluated. The final description of the motion of the material points of the heart is a four-dimensional B-spline forward motion field:

$$\phi(\bar{P}, t) = \sum_u \sum_v \sum_w \sum_t B_u(\tilde{x}) B_v(\tilde{y}) B_w(\tilde{z}) B_t(t) \cdot \vec{C}_{u,v,w,t}. \quad (6)$$

The accuracy of the final forward motion field can be evaluated with the forward field residual error, which is the 3-D distance between the original tag point and the posi-

Strain imaging with MRI tagging now gives us a new tool for studying the temporal kinetics of myocardial contraction.

tion to which that tag point is mapped following its inverse and forward transformations.

Strain Calculation

Equation (6) represents a parametric representation of the material coordinate displacement field. The displacement gradient can be computed at each point

$$\mathcal{J}(\tilde{x}, \tilde{y}, \tilde{z}) = \begin{bmatrix} \frac{\partial \phi_x}{\partial \tilde{x}} & \frac{\partial \phi_y}{\partial \tilde{x}} & \frac{\partial \phi_z}{\partial \tilde{x}} \\ \frac{\partial \phi_x}{\partial \tilde{y}} & \frac{\partial \phi_y}{\partial \tilde{y}} & \frac{\partial \phi_z}{\partial \tilde{y}} \\ \frac{\partial \phi_x}{\partial \tilde{z}} & \frac{\partial \phi_y}{\partial \tilde{z}} & \frac{\partial \phi_z}{\partial \tilde{z}} \end{bmatrix} \quad (7)$$

where ϕ_i is the i th component of the material displacement field as calculated by (6). Equation (6) can be differentiated directly using properties of the B-spline basis function. For example:

$$\mathcal{J}_{\tilde{x}, \tilde{x}} = \sum_u \sum_v \sum_w \sum_t B'_u(\tilde{x}) B_v(\tilde{y}) B_w(\tilde{z}) B_t(t) \cdot C'_{u,v,w,t} \quad (8)$$

where B' is the derivative of the B-spline basis function. The derivative of a cubic B-spline with a knot sequence

$$K = \{0, 0, 0, 0, u_1, \dots, u_k, \dots, u_{k-3}, 1, 1, 1, 1\}$$

$$\text{where } u_n = \frac{n}{k-2} \text{ for } 1 \leq n \leq (k-3)$$

can be calculated directly as the quadratic B-spline of the shortened knot sequence:

$$K' = \{0, 0, 0, u_1, \dots, u_k, \dots, u_{k-3}, 1, 1, 1\}$$

$$\text{where } u_n = \frac{n}{k-2} \text{ for } 1 \leq n \leq (k-3).$$

The tensor product for the desired displacement gradient component for the whole space is done as before with the difference that the basis in the \tilde{x} direction is now quadratic. The new control points can be computed from the old ones as

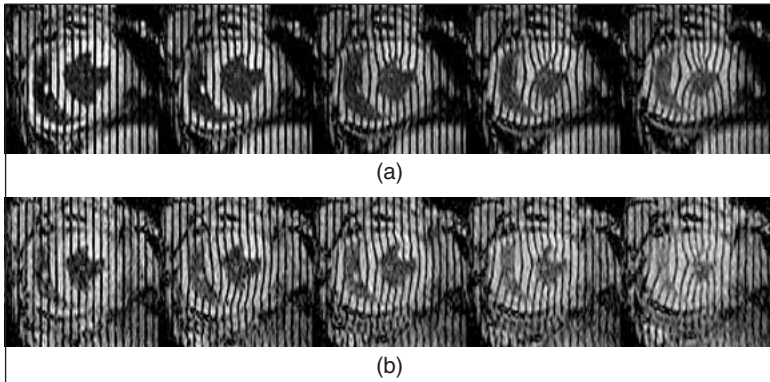
$$C'_{u,v,w,t} = p \frac{C_{u+1,v,w,t} - C_{u,v,w,t}}{K_{i+p+1} - K_{i+1}} \quad (9)$$

where p is the degree of the B-spline ($p=3$ for our case), and K is the original knot sequence in the \tilde{x} direction. The

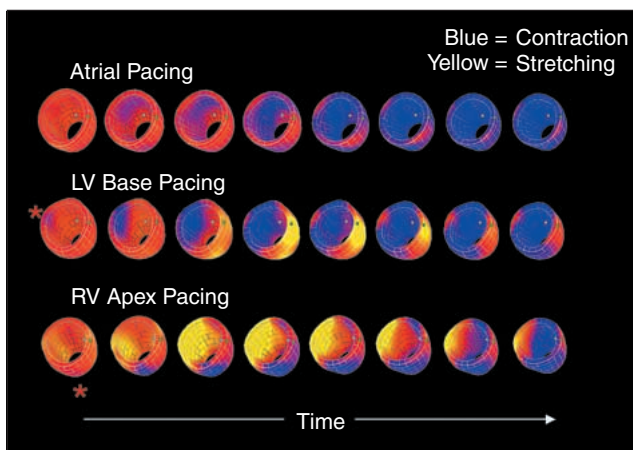
remaining eight components of the displacement gradient tensor can be similarly described analytically. The local Lagrangian strain tensor at any location [64], E , can then be computed from the displacement gradient, \mathcal{G} , using the formula

$$E = \frac{1}{2} (\mathcal{G}^T + \mathcal{G} + \mathcal{G}^T \mathcal{G}). \quad (10)$$

After it is computed, the strain can be transformed to a local surface-based coordinate system to display circumferential, longitudinal, and radial components, corresponding to the more physiological parameters of circumferential and longitudinal muscle shortening, and radial wall thickening.



▲ 8. The effect of ventricular pacing on the timing of myocardial contraction. The top row shows a sequence of movie frames in a contracting heart after pacing from the right atrium. This leads to a normal synchronous activation and symmetric contraction pattern. The bottom row shows the same heart when paced from the right ventricular apex. Notice the early contraction of the septum (about 9 o'clock) and the bulging back of the lateral free wall (3 o'clock).



▲ 9. Strain images in a single heart for three pacing conditions. Contraction is shown as blue, and stretching is shown as yellow. When paced at the atrium contraction is coherent in space and time. When the ventricle is paced from the LV free wall (asterisk), the contraction begins at the pacing site and spreads around the LV. There is significant prestretch on the heart wall opposite the pacing site. When the heart is paced from the RV apex (bottom row) the pattern is the same, but the origin of the contraction wave is moved to the new pacing site. Images like these can be used to locate the origin of ectopic excitation.

Analysis of Myocardial Function During Asynchronous Activation

In the normal heart electrical activation spreads over the left ventricle (LV) rapidly through a specialized conduction system, which produces a coherent contraction of heart muscle fibers. A disruption of the timing in this normal contraction pattern is often the hallmark of cardiac disease. A noninvasive imaging method for measuring the timing of mechanical contraction would allow the evaluation of pathologies such as bundle branch block and Wolff-Parkinson-White syndrome [57], or the evaluation of ectopic excitation of the ventricle by a pacemaker [9], [48], [59]. While asynchronous activation has been observed before with nuclear medicine [10] and direct video imagery of physical markers on the heart wall [59], MR tagging is the only imaging method able to resolve the local contraction of the heart wall over the entire heart. While externally pacing the heart and sensing the electrocardiogram during MRI presents a challenge because of the voltages induced in the pacing leads by the radio-frequency (RF) pulses and the magnetic field gradient pulses, specialized filters can be designed to eliminate these voltages [34], [65], [66].

Experimental Setup for Imaging Mechanical Activation During Ectopic Pacing

To evaluate the relationship between electrical excitation and the onset of mechanical contraction, MR tagging experiments were performed during ectopic pacing in anesthetized normal dogs [45], [69]. (The experiments were performed in accordance with the guidelines set by the Johns Hopkins Animal Care and Use Committee, and The Animal Care and Use Committee of the NIH.) One pacing lead was sewn onto the right atrium to create normal activation of the heart through the HIS-Purkinje system. Also, two ventricular pacing sites were investigated: the right ventricular apex, which is the normal position for a pacemaker lead placed chronically, and the left ventricular basal free wall. The leads were connected to the pacing and monitoring system through filter connectors on the penetration panel of the RF-shielded scanning room. The electrical stimulation pulses to pace the heart were generated by a GRASS stimulator and passed through isolation units, and the specially designed RF filter units before being delivered to the pacing leads on the heart.

If systolic contraction is evoked by right atrial pacing, the LV is excited via the normal pathway of the Purkinje system and the pattern of mechanical activation is found to be very uniform as a function of position. When the heart is paced from a ventricular site, however, significant asynchronous and spatially heterogeneous contraction is observed. The abnormal contraction pattern associated

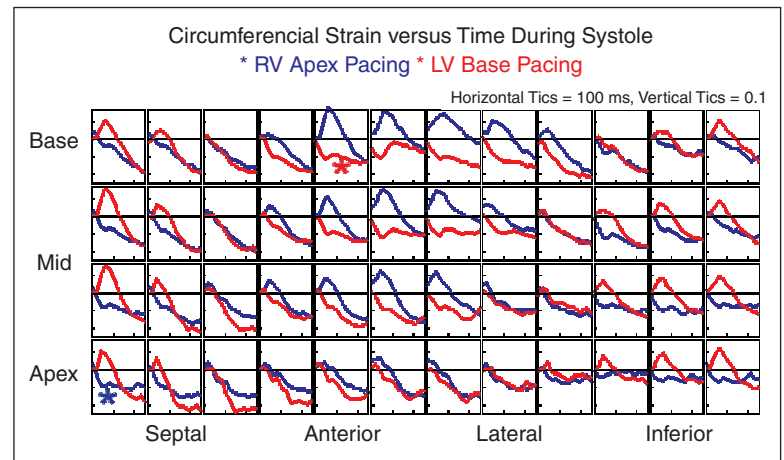
with ventricular pacing is immediately obvious when the sequences of tagged MR images are viewed in a movie loop. Fig. 8 shows a sequence of short axis tagged MR images in a mid-ventricular slice when paced from the right atrial appendage and also the right ventricular apex. The asynchrony in the contraction of the myocardium during ventricular pacing is clearly demonstrated in this figure by the asymmetric deformation of the tag lines during systole.

The precise sequence of events during ectopic excitation is clearly evident on the strain images. Fig. 9 shows the evolution in time of the circumferential component of the 3-D strain tensor (E_{α}) evaluated at the mid-wall for the three pacing sites; this component of the strain tensor closely matches muscle fiber shortening at the mid-wall of the LV. For atrial pacing (normal activation pathway) muscle shortening evolves relatively homogeneously over the ventricle; this is shown as the uniformly increasing blue color over the ventricle in the top row of Fig. 9. With ventricular pacing, a clear focus of early mechanical activation is observed at the pacing site, followed by propagation of a contraction wave-front to the opposite side of the heart. This is seen as the blue “wave” of muscle shortening emanating from the LV freewall pacing site (10 o’clock) in the middle row of Fig. 9 and from the right ventricular apex site (5 o’clock) in the bottom row of Fig. 9. A second interesting observation was the significant “prestretch” of the late activated myocardium remote from the pacing site. This prestretch was quite pronounced (15-20%) and occurred in the first 100 ms after the ventricular pacing pulse. This prestretch is shown as the bright yellow color in the strain images of Fig. 9 and arises because the early activated tissue generates pressure in the LV which pushes against the noncontracting late activated tissue.

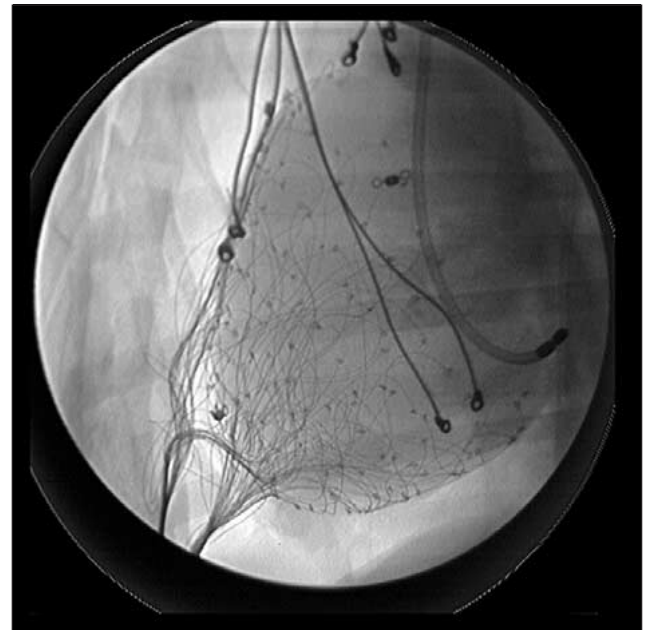
An alternative way of visualizing the contraction pattern is to graph the time course of strain for each material point of the heart. Each graph can be mapped to a position in an array that corresponds to a position in the heart. An example of such a *strain map* is shown in Fig. 10 where the sequence of mechanical shortening (mid-wall E_{α}) for the left ventricular base and right ventricular apex pacing sites are plotted. The strain maps are an excellent method for observing the rapid rate of prestretch in the passive, late activated regions (see columns 1-2 and 11-12 for LV base pacing, columns 4-9 for right ventricular apex pacing) and the rapid contraction at the pacing site (columns 5-6 for LV base pacing, columns 1-2 for right ventricular apex pacing). Also demonstrated directly from these plots is the increased stroke or total dynamic range of the strain in the prestretched region. Because the majority of this shortening occurs during the ejection phase (with high

ventricular pressure), the prestretched region is performing increased contractile work [24], [60]. This concept of work redistribution may have an impact in the choice of pacing paradigms for therapy.

Asynchronous mechanical activation is obvious from both the color encoded strain images shown in Fig. 9 and the strain maps showing E_{α} versus time in Fig. 10. It is



▲ 10. Curves showing the circumferential strain versus time for two pacing locations. This component of the strain tensor is the same as myocardial shortening, or contraction, during normal systolic contraction of the ventricles. The red curves show circumferential strain after pacing the heart at the LV base (the pacing location is shown as an asterisk). The strain curves show immediate contraction in the region around the pacing lead; however, the regions on the opposite wall of the heart (for example, the boxes in the first column of this map) show a significant prestretch (positive strain) before they begin to contract. The time of the onset of contraction can be determined from the peak of the prestretch curve.



▲ 11. A fluoroscopic X-ray image of the electrode sock surrounding the heart. The large dark leads with the circular ends are bipolar pacing leads sewn onto the epicardial surface. A registration marker is visible at 12 o’clock, approximately 1/3 of the way down from the top, and a pacing catheter is also visible between 1 o’clock and 3 o’clock.

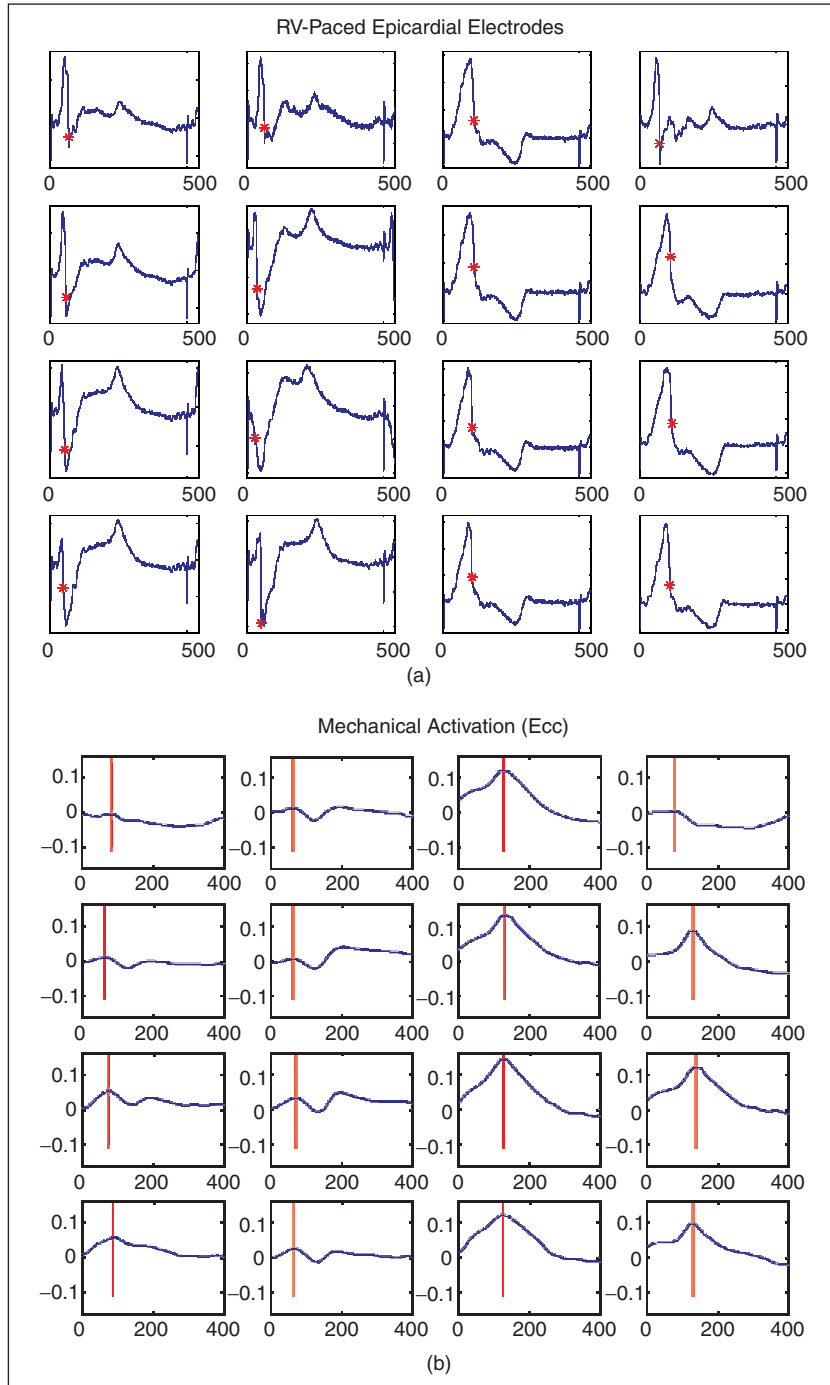
also clear that the spatial origin of activation is visible, therefore we should be able to accurately map the onset of contraction; this parameter could be used for localization of ectopic foci in the heart. If we define the mechanical activation time as the time at which the muscle begins to shorten, this will correspond to the time at which the prestretch or ventricular filling reaches a peak, as shown in the strain maps of Fig. 10. Not all of the curves in Fig

10 have peaks because in this case MR imaging commenced directly after pacing the heart; however, it is possible to begin the MR acquisition before the heart has completed filling, and before the pacing stimulus, to provide a positive E_{α} strain peak at all locations.

The mechanical data described above can be obtained from a dog *in vivo* while simultaneously measuring epicardial electrical excitation maps with an electrode array placed around the heart. Such an electrode array surrounding the ventricles is shown in a fluoroscopic view in Fig. 11.

The electrical signals are carried out of the MRI scan room through the appropriate filters to eliminate contamination of the signal from the MR scanner. Surprisingly, even though there is a remarkable amount of fine copper wire surrounding the heart, the MR image quality is not degraded in the myocardium by the presence of the electrode sock; the only visible artifacts are very small dark spots on the epicardial surface. Fig. 12(a) shows a subset of the 128 unipolar electrical traces measured on the epicardial surface with the dog in the MR scanner; Fig. 12(b) shows a set of E_{α} versus time graphs for the same heart, obtained immediately after the electrical measurements were made.

From the data shown in Fig. 12, maps of both mechanical activation (time of onset of shortening) and electrical activation (time of maximum negative slope in unipolar recordings) were computed. Color encoded activation maps superimposed on the 3-D coordinates of the epicardial surface of the heart are shown in Fig. 13. There is a high degree of correlation between the electrical activation map and the mechanical activation map, as it is defined here. This is not surprising in the normal heart where electrical depolarization of the cells is the signaling event for the release of calcium and the beginning of contraction. The change in the nature of this dependence in pathology, such as regional ischemia, and during administration of drugs that affect electrical–calcium coupling and myocyte ion channels is just now under investigation.



▲ 12. (a) Unipolar epicardial electrode measurements obtained *in vivo*, inside the MR scanner. The time of depolarization is marked with an asterisk (time of maximum negative derivative). (b) Circumferential component of the strain tensor measured in the same heart with MR tagging. The mechanical activation time, chosen as the peak prestretch or filling is shown as a vertical red line.

Clinical Application

Ventricular pacing has been demonstrated to immediately reduce ventriculo-aortic pressure gradients in hypertrophic obstructive cardiomyopathy [18], [28], [29], [37], and these improvements can be long

term [29]. Also, recent studies have begun to explore the potential for enhancing cardiac function in patients with dilated cardiomyopathy (DCM), a form of heart failure, by altering the ventricular activation sequence [6], [11], [38]. The principle behind this therapy is that profound dyssynchrony exists in some patients with DCM and restoration of a more coherent activation will increase function. Fig. 14 shows a side-by-side comparison between the mechanical activation of a normal left ventricle and that of a patient in end stage dilated cardiomyopathy [21]. While the normal LV shows a coherent onset of shortening, the DCM patient shows septal activation first (right side of LV), followed by late free-wall activation. The measurement of the location of this late activation in the heart can be used to plan the appropriate location of a pacing stimulus to resynchronize the heart.

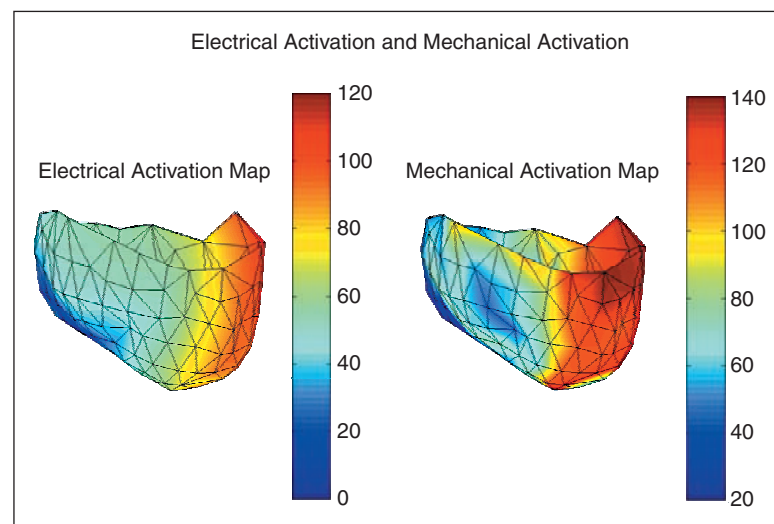
The patient shown in this example responded very well to ventricular free-wall pacing. Ventricular pacing was achieved at the LV base in the epicardium by placing a coronary sinus catheter at the origin of an anterior wall vein. With LV pacing, there was a near *doubling* of stroke volume and thus cardiac output (since heart rate was constant), even though the QRS complex became much wider than at baseline. The patient reported feeling his heart pounding in his chest, consistent with the enhancement of systolic function.

Discussion

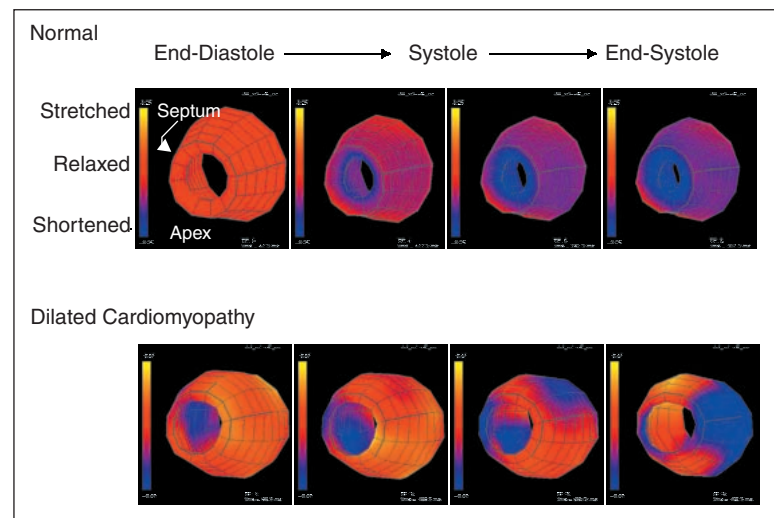
Strain imaging with MRI tagging now gives us a new tool for studying the temporal kinetics of myocardial contraction. Because this technique is noninvasive, it can be applied in patients with no risk. Under conditions where the heart is beating in a reproducible manner, high resolution mechanical activation maps can be achieved, and these will correlate with the underlying electrical activation. The strain imaging data could possibly be used as a further boundary condition with torso ECG data to perform more accurate reconstruction of epicardial electrophysiological maps from body surface potentials [42]. One direction of research that is now possible is the study of the effect of mechanical stretch on the electrical nature of the heart. It has been demonstrated that rapid prestretch will stimulate depolarization of the myocardium especially in regions that have the greatest compliance and experience greater relative stretch [31], and that the timing of the application of prestretch determines if an arrhythmic depolarization of the

The speed of MRI acquisition has increased dramatically with the advent of improved scanner hardware.

LV will occur [72]. This new strain imaging technique combined with simultaneous electrical mapping will allow us to investigate the local prestretch needed to generate these arrhythmic beats.



▲ 13. An electrical activation map and a mechanical activation map obtained on the same heart. The color mapped onto these models represents activation time. For both of the above figures, the heart was paced at the RV apex, which is the site of earliest activation (blue color). The wave of electrical depolarization moves across the heart to the LV free wall (right side of 3-D model), and the mechanical activation tracks behind it.



▲ 14. Comparison of myocardial strain images from a normal left ventricle (top row) and a left ventricle of a patient with dilated cardiomyopathy (bottom row). In the patient, the early contraction of the septum (9 o'clock) is evident, with late contraction of the LV free wall (3 o'clock).

Acknowledgments

Much of the work discussed in this article was supported through grants from the NHLBI (HL45090, HL45683), the Whitaker Foundation, the Radiological Society of North America, and the American Heart Association. Many of the results and conclusions reported here are from the collaborative efforts of the Cardiac MRI Research Group at Johns Hopkins. We would especially like to acknowledge the efforts of Cecilia Curry, Jerome Declerck, Owen Faris, Michael Guttman, Chris Moore, Walter O'Dell, Scott Reeder, Frits Prinzen, Bradley Wyman, Joni Taylor, Joshua Tsitlik, Henry Halperin, William Hunter, and Elias Zerhouni. All of our electrical mapping techniques were taught to us by Bob Lux and Rob McLeod at CVRTI, University of Utah. The derivation of the B-spline method for tag tracking is from C. Ozturk. The clinical example was done in collaboration with David Kass.

Elliot McVeigh received his bachelor's degree in physics in 1984 and his Ph.D. in medical biophysics in 1988, both from the University of Toronto. Since then he has been active in the development of new techniques in cardiac MRI, first as faculty at the Johns Hopkins University School of Medicine in Baltimore and now as a Principal Investigator at the National Heart Lung and Blood Institute in Bethesda.

Cengizhan Ozturk earned his M.D. from Marmara School of Medicine, Istanbul, Turkey, in 1990. He proceeded with a specialization in physiology from Cerrahpasa Medical School, Istanbul, in 1994 and a Ph.D. at the School of Biomedical Engineering, Science and Health Systems, Drexel University, Philadelphia, in 1997. During 1997-2000, he worked as a postdoctoral research fellow in the Medical Imaging Lab, Department of Biomedical Engineering, Johns Hopkins University School of Medicine. His main research area is the development of new methods for rapid physiologic evaluation and tissue tracking for cardiac MRI images, evaluation of right ventricular function, atrial motion, and the development of a four-chamber motion field. He is currently an Assistant Professor at the Institute of Biomedical Engineering, Bogazici University, Istanbul, Turkey.

References

- [1] A.H. Aletras, R.S. Balaban, and H. Wen, "High-resolution strain analysis of the human heart with fast-DENSE," *J. Magn. Reson.*, vol. 140, pp. 41-57, 1999.
- [2] American Heart Association, "2001 heart and stroke statistical update," American Heart Association, Dallas, TX, 2000.
- [3] A.A. Amini, A.Y. Chen, R.W. Curwen, and V.S.J. Mani, "Coupled B-snake grids and constrained thin-plate splines for analysis of 2-D tissue deformations from tagged MRI," *IEEE Trans. Med. Imag.*, vol. 17, pp. 344-356, 1998.
- [4] E. Atalar and E.R. McVeigh, "Optimum tag thickness for the measurement of position with MRI," *IEEE Trans. Med. Imag.*, vol. 13, pp. 152-160, 1994.
- [5] D.J. Atkinson and R.R. Edelman, "Cineangiography of the heart in a single breath hold with a segmented turboflash sequence," *Radiology*, vol. 178, pp. 357-360, 1991.
- [6] A. Auricchio, C. Stellbrink, M. Block, S. Sack, J. Vogt, P. Bakker, H. Klein, A. Kramer, J. Ding, R. Salo, B. Tockman, T. Pochet, and J. Spinelli, "Effect of pacing chamber and atrioventricular delay on acute systolic function of paced patients with congestive heart failure. The pacing therapies for congestive heart failure study group. The guidant congestive heart failure research group," *Circulation*, vol. 99, pp. 2993-3001, 1999.
- [7] L. Axel and L. Dougherty, "Heart wall motion: Improved method of spatial modulation of magnetization for MR imaging," *Radiology*, vol. 172, pp. 349-360, 1989.
- [8] L. Axel and L. Dougherty, "MR imaging of motion with spatial modulation of magnetization," *Radiology*, vol. 171, pp. 841-845, 1989.
- [9] F.R. Badke, P. Boinay, and J.W. Covell, "Effects of ventricular pacing on regional left ventricular performance in the dog," *Amer. J. Physiol.*, vol. 238, pp. H858-H867, 1980.
- [10] T.M. Bashore, R.A. Stine, P.B. Shaffer, C.A. Bush, C.V. Leier, and S.F. Schaal, "The noninvasive localization of ventricular pacing sites by radionuclide phase imaging," *Circulation*, vol. 70, pp. 681-694, 1984.
- [11] J.J. Blanc, Y. Etienne, M. Gilard, et al., "Evaluation of different ventricular pacing sites in patients with severe heart failure: Results of an acute hemodynamic study," *Circulation*, vol. 96, pp. 3273-3277, 1997.
- [12] B. Bolster, E.R. McVeigh, J. Shoener, and E.A. Zerhouni, "Efficient production of high resolution tagging grids with sinc modulated comb functions," in *Soc. of Magn. Reson. in Med., Book of Abstracts*. New York: Wiley-Liss, 1990, vol. 3, p. 1115.
- [13] B.D. Bolster, Jr., E.R. McVeigh, and E.A. Zerhouni, "Myocardial tagging in polar coordinates with use of striped tags," *Radiology*, vol. 177, pp. 769-772, 1990.
- [14] P.A. Bottomley, C.H. Lugo Olivier, and R. Giaquinto, "What is the optimum phased array coil design for cardiac and torso magnetic resonance?" *Magn. Reson. Med.*, vol. 37, pp. 591-599, 1997.
- [15] W.A. Boxley and T.J. Reeves, "Abnormal regional myocardial performance in coronary artery disease," *Prog. Cardiovasc. Dis.*, vol. 13, pp. 405-421, 1971.
- [16] D.H. Brooks and R.S. MacLeod, "Electrical imaging of the heart," *IEEE Signal Processing Mag.*, vol. 14, pp. 24-42, 1997.
- [17] J.E. Burnes, B. Taccardi, and Y. Rudy, "A noninvasive imaging modality for cardiac arrhythmias," *Circulation*, vol. 102, pp. 2152-2158, 2000.
- [18] R.O. Cannon, D. Tripodi, V. Dilsizian, J.A. Panza, and L. Fananapazir, "Results of permanent dual-chamber pacing in symptomatic nonobstructive hypertrophic cardiomyopathy," *Amer. J. Cardiol.*, vol. 73, pp. 571-576, 1994.
- [19] C.D. Constantinides, E. Atalar, and E.R. McVeigh, "Signal-to-noise measurements in magnitude images from NMR phased arrays," *Magn. Reson. Med.*, vol. 38, pp. 852-857, 1997.
- [20] C.D. Constantinides, C.R. Westgate, W.G. O'Dell, E.A. Zerhouni, and E.R. McVeigh, "A phased array coil for human cardiac imaging," *Magn. Reson. Med.*, vol. 34, pp. 92-98, 1995.
- [21] C.W. Curry, G.S. Nelson, B.T. Wyman, J. Declerck, M. Talbot, R.D. Berger, E.R. McVeigh, and D.A. Kass, "Mechanical dyssynchrony in dilated cardiomyopathy with intraventricular conduction delay as depicted by 3D tagged magnetic resonance imaging," *Circulation*, vol. 101, p. E2, 2000.
- [22] C. de Boor, *A Practical Guide to Splines*. Springer-Verlag, 1978.
- [23] J. Declerck, T.S. Denney, C. Ozturk, W. O'Dell, and E.R. McVeigh, "Left ventricular motion reconstruction from planar tagged MR images: A comparison," *Phys. Med. Biol.*, vol. 45, pp. 1611-1632, 2000.

- [24] T. Delhaas, T. Arts, F.W. Prinzen, and R.S. Reneman, "Regional fibre stress-fibre strain area as an estimate of regional blood flow and oxygen demand in the canine heart," *J. Physiol.*, vol. 477, pp. 481-496, 1994.
- [25] T.S. Denney and E.R. McVeigh, "Model-free reconstruction of three-dimensional myocardial strains from planar tagged MR images," *J. Magn. Reson. Imag.*, vol. 7, pp. 799-810, 1997.
- [26] A.S. Douglas, E.K. Rodriguez, W. O'Dell, and W.C. Hunter, "Unique strain history during ejection in canine left ventricle," *Amer. J. Physiol.*, vol. 260, pp. H1596-H1611, 1991.
- [27] F.H. Epstein, S.D. Wolff, and A.E. Arai, "Segmented k-space fast cardiac imaging using an echo-train readout," *Magn. Reson. Med.*, vol. 41, pp. 609-613, 1999.
- [28] L. Fananapazir, R.O. Cannon, D. Tripodi, and J.A. Panza, "Impact of dual-chamber permanent pacing in patients with obstructive hypertrophic cardiomyopathy with symptoms refractory to verapamil and beta-adrenergic blocker therapy," *Circulation*, vol. 85, pp. 2149-2161, 1992.
- [29] L. Fananapazir, N.D. Epstein, R.V. Curiel, J.A. Panza, D. Tripodi, and D. McAreevey, "Long-term results of dual-chamber (ddd) pacing in obstructive hypertrophic cardiomyopathy. Evidence for progressive symptomatic and hemodynamic improvement and reduction of left ventricular hypertrophy," *Circulation*, vol. 90, pp. 2731-2742, 1994.
- [30] S.E. Fischer, G.C. McKinnon, S.E. Maier, and P. Boesiger, "Improved myocardial tagging contrast," *Magn. Reson. Med.*, vol. 30, pp. 191-200, 1993.
- [31] M.R. Franz, R. Cima, D. Wang, D. Profitt, and R. Kurz, "Electrophysiological effects of myocardial stretch and mechanical determinants of stretch-activated arrhythmias," *Circulation*, vol. 86, pp. 968-978, 1992.
- [32] M.A. Guttman, J.L. Prince, and E.R. McVeigh, "Tag and contour detection in tagged MR images of the left ventricle," *IEEE Trans. Med. Imag.*, vol. 13, pp. 74-88, 1994.
- [33] E.M. Haacke, R.W. Brown, M.R. Thompson, and R. Venkatesan, *Magnetic Resonance Imaging: Physical Principles and Sequence Design*. New York: Wiley, 1999.
- [34] H.R. Halperin, H.R. Levin, E.R. McVeigh, P. Cho, W. Curtis, C. Moore, M. Acker, J.E. Tsitlik, and P. Belfer, "New techniques for the study of cardiomyoplasty," in *Proc. Ann. Int. Conf. IEEE Engineering in Medicine and Biology Soc.*, 1992, vol. 14, pp. 2794-2795.
- [35] D.E. Hansen, G.T. Daughters, E.L. Alderman, N.B. Ingels, E.B. Stinson, and D.C. Miller, "Effect of volume loading, pressure loading, and inotropic stimulation on left ventricular torsion in humans," *Circulation*, vol. 83, pp. 1315-1326, 1991.
- [36] M.V. Herman and R. Gorlin, "Implications of left ventricular asynergy," *Amer. J. Cardiol.*, vol. 23, pp. 538-547, 1969.
- [37] X. Jeanrenaud, J.J. Goy, and L. Kappenberger, "Effects of dual-chamber pacing in hypertrophic obstructive cardiomyopathy," *Lancet*, vol. 339, pp. 1318-1323, 1992.
- [38] D.A. Kass, C.H. Chen, C. Curry, M. Talbot, R. Berger, B. Fetis, and E. Nevo, "Improved left ventricular mechanics from acute VDD pacing in patients with dilated cardiomyopathy and ventricular conduction delay," *Circulation*, vol. 99, pp. 1567-1573, 1999.
- [39] D.L. Kraitchman, L. Axel, and A.A. Young, "Springs: A fast method for detection and correspondence of cardiac magnetic resonance tags," *Soc. of Magn. Reson. in Med., Book of Abstracts*. New York: Wiley-Liss, 1993, vol. 2, p. 725.
- [40] Z.P. Liang and P.C. Lauterbur, *Principles of Magnetic Resonance Imaging: A Signal Processing Perspective*. Piscataway, NJ: IEEE Press, 2000.
- [41] Z.W. Liu, P. Jia, L.A. Biblo, B. Taccardi, and Y. Rudy, "Endocardial potential mapping from a noncontact nonexpandable catheter: A feasibility study," *Ann. Biomed. Eng.*, vol. 26, pp. 994-1009, 1998.
- [42] R.S. MacLeod and D.H. Brooks, "Recent progress in inverse problems in electrocardiology," *IEEE Eng. Med. Biol. Mag.*, vol. 17, pp. 73-83, 1998.
- [43] B. Madore, G.H. Glover, and N.J. Pelc, "Unaliasing by fourier-encoding the overlaps using the temporal dimension (UNFOLD), applied to cardiac imaging and fMRI," *Magn. Reson. Med.*, vol. 42, pp. 813-828, 1999.
- [44] E.R. McVeigh and E. Atalar, "Cardiac tagging with breath-hold cine MRI," *Magn. Reson. Med.*, vol. 28, pp. 318-327, 1992.
- [45] E.R. McVeigh, F.W. Prinzen, B.T. Wyman, J.E. Tsitlik, H.R. Halperin, and W.C. Hunter, "Imaging asynchronous mechanical activation of the paced heart with tagged MRI," *Magn. Reson. Med.*, vol. 39, pp. 507-513, 1998.
- [46] E.R. McVeigh and E.A. Zerhouni, "A rapid starburst sequence for cardiac tagging," *Soc. of Magn. Reson. in Med., Book of Abstracts*. New York: Wiley-Liss, 1989, vol. 1, p. 23.
- [47] E.R. McVeigh and E.A. Zerhouni, "Noninvasive measurement of transmural gradients in myocardial strain with magnetic resonance imaging," *Radiology*, vol. 180, pp. 677-683, 1991.
- [48] K. Miyazawa, T. Honma, T. Haneda, K. Shirato, T. Nakajima, and T. Arai, "Dynamic geometry of the left ventricle during ventricular pacing: Correlation with cardiac pumping action," *Toboku J. Exp. Med.*, vol. 124, pp. 261-266, 1978.
- [49] C.C. Moore, E.R. McVeigh, A. Mebazaa, and E.A. Zerhouni, "Use of striped radial tagging to measure three-dimensional endocardial and epicardial deformation throughout the canine left ventricle during ischemia," *J. Magn. Reson. Imag.*, vol. 3, p. 124, 1993.
- [50] C.C. Moore, S.B. Reeder, and E.R. McVeigh, "Tagged MR imaging in a deforming phantom-photographic validation," *Radiology*, vol. 190, pp. 765-769, 1994.
- [51] O.C. Morse and J.R. Singer, "Blood velocity measurement in intact subjects," *Science*, vol. 170, pp. 440-441, 1970.
- [52] T.J. Mosher and M.B. Smith, "A DANTE tagging sequence for the evaluation of translational sample motion," *Magn. Reson. Med.*, vol. 15, pp. 334-339, 1990.
- [53] W.G. O'Dell, C.C. Moore, W.C. Hunter, E.A. Zerhouni, and E.R. McVeigh, "Displacement field fitting for calculating 3D myocardial deformations from tagged MR images," *Radiology*, vol. 195, pp. 829-835, 1995.
- [54] W.G. O'Dell, C.C. Moore, and E.R. McVeigh, "Displacement field fitting approach to calculate 3D deformations from parallel-tagged MR images," *J. Magn. Reson. Imag.*, vol. 3, p. 208, 1993.
- [55] N.F. Osman, W.S. Kerwin, E.R. McVeigh, and J.L. Prince, "Cardiac motion tracking using CINE harmonic phase (HARP) magnetic resonance imaging," *Magn. Reson. Med.*, vol. 42, pp. 1048-1060, 1999.
- [56] C. Ozturk and E.R. McVeigh, "Four-dimensional B-spline based motion analysis of tagged MR images: Introduction and in vivo validation," *Phys. Med. Biol.*, vol. 45, pp. 1683-1702, 2000.
- [57] W.J. Parks, R.I. Pettigrew, T.D. Ngo, E. Hulse, and R. Campbell, "Identification of Preexcitation sites in Wolff-Parkinson-White syndrome using magnetic tagging," *Soc. Magn. Reson. Med., Book of Abstracts*, vol. 1, p. 274, 1993.
- [58] N.J. Pelc, R.J. Herfkens, A. Shimakawa, and D.R. Enzmann, "Phase contrast cine magnetic resonance imaging," [review], *Magn. Reson. Quart.*, vol. 7, pp. 229-254, 1991.
- [59] F.W. Prinzen, C.H. Augustijn, T. Arts, M.A. Allessie, and R.S. Reneman, "Redistribution of myocardial fiber strain and blood flow by asynchronous activation," *Amer. J. Physiol.*, vol. 259, pp. H300-H308, 1990.
- [60] F.W. Prinzen, W.C. Hunter, B.T. Wyman, and E.R. McVeigh, "Mapping of regional myocardial strain and work during ventricular pacing: Experimental study using magnetic resonance imaging tagging," *J. Amer. Coll. Cardiol.*, vol. 33, pp. 1735-1742, 1999.
- [61] K.P. Pruessmann, M. Weiger, M.B. Scheidegger, and P. Boesiger, "SENSE: Sensitivity encoding for fast MRI," *Magn. Reson. Med.*, vol. 42, pp. 952-962, 1999.

- [62] S.B. Reeder, E. Atalar, A.Z. Faranesh, and E.R. McVeigh, "Multi-echo segmented k-space imaging: An optimized hybrid sequence for ultrafast cardiac imaging," *Magn. Reson. Med.*, vol. 41, pp. 375-85, 1999.
- [63] G. Salama, "Optical measurement of transmembrane potential," in *Spectroscopic Membrane Probes*, L. Loew, Ed. Boca Raton, FL: CRC, 1988, vol. III, pp. 137-199.
- [64] A.J.M. Spencer, *Continuum Mechanics*. White Plains, NY: Longman, 1980.
- [65] J.E. Tsitlik, H.E. Levin, E.R. McVeigh, W. Rogers, L. Perry, and H. Halperin, "Safe and reliable pacing in dogs during MRI in a 1.5 T magnet," *iPACE* 15, vol. II, 1992, pp. 561-561.
- [66] J.E. Tsitlik, H.R. Levin, A. Herskowitz, E.R. McVeigh, C.C. Moore, and H.R. Halperin, "Magnetic resonance imaging-induced myocardial injury can be prevented during cardiac pacing," *iPACE*, vol. 18, 1995, p. 830.
- [67] L.K. Waldman, Y.C. Fung, and J.W. Covell, "Transmural myocardial deformation in the canine left ventricle," *Circulation Res.*, vol. 57, pp. 152-163, 1985.
- [68] V.J. Wedeen, "Magnetic resonance imaging of myocardial kinematics: Technique to detect, localize, and quantify the strain rates of the active human myocardium," *Magn. Reson. Med.*, vol. 27, pp. 52-67, 1992.
- [69] B.T. Wyman, W.C. Hunter, F.W. Prinzen, and E.R. McVeigh, "Mapping propagation of mechanical activation in the paced heart with MRI tagging," *Amer. J. Physiol.*, vol. 276, pp. H881-H891, 1999.
- [70] A.A. Young and L. Axel, "Three-dimensional motion and deformation of the heart wall: Estimation with spatial modulation of magnetization—A model-based approach," *Radiology*, vol. 185, pp. 241-247, 1992.
- [71] A.A. Young, L. Axel, L. Dougherty, D.K. Bogen, and C.S. Parenteau, "Validation of tagging with MR imaging to estimate material deformation," *Radiology*, vol. 188, pp. 101-108, 1993.
- [72] M. Zabel, B.S. Koller, F. Sachs, and M.R. Franz, "Stretch-induced voltage changes in the isolated beating heart: Importance of the timing of stretch and implications for stretch-activated ion channels," *Cardiovasc. Res.*, vol. 32, pp. 120-130, 1996.
- [73] E.A. Zerhouni, D.M. Parish, W.J. Rogers, A. Yang, and E.P. Shapiro, "Human heart: Tagging with MR imaging—A method for noninvasive assessment of myocardial motion," *Radiology*, vol. 169, pp. 59-63, 1988.